International Journal of Nanomedicine

Dovepress
Taylor & Francis Group

Open Access Full Text Article

ORIGINAL RESEARCH

Targeted Delivery of BMS-1166 for Enhanced Breast Cancer Immunotherapy

Zhecheng Yu[1–4], Zeya Zhou[1–4], Yunqi Zhao[1–4]

[1]College of Science, Mathematics and Technology, Wenzhou-Kean University, Wenzhou, Zhejiang, People's Republic of China; [2]Wenzhou Municipal Key Laboratory for Applied Biomedical and Biopharmaceutical Informatics, Wenzhou-Kean University, Wenzhou, Zhejiang, People's Republic of China; [3]Zhejiang Bioinformatics International Science and Technology Cooperation Center, Wenzhou-Kean University, Wenzhou, Zhejiang, People's Republic of China; [4]Dorothy and George Hennings College of Science, Mathematics and Technology, Kean University, Union, NJ, USA

Correspondence: Yunqi Zhao, College of Science, Mathematics and Technology, Wenzhou-Kean University, Wenzhou, Zhejiang, People's Republic of China, Tel +86 577 5587 0000, Fax +86 577 5587 0101, Email yuzhao@kean.edu

Background: Cancer immunotherapy has achieved great success in breast cancer treatment in recent years. The Programmed Death-1 (PD-1) /Programmed Death-Ligand 1 (PD-L1) immune checkpoint pathway is among the most studied. BMS-1166, a PD-L1 inhibitor, can interfere with PD-1 and PD-L1 interaction. Transferrin Receptor 1 is a transmembrane glycoprotein overexpressed in various cancer cells, including breast cancer, and can specifically interact with the T7 (HAIYPRH) peptide.

Purpose: This study hypothesized that BMS-1166-loaded T7-modified poly(ethylene glycol)-poly(ε-caprolactone) (PEG-PCL) polymeric micelles (BMS-T7) could block PD-L1 interaction with PD-1, serving as a targeted immunotherapy for TfR1-positive breast cancer.

Methods: BMS-1166 was encapsulated in T7-PEG-PCL micelle. Particle size and zeta potential were determined by dynamic light scattering. Particle morphology was studied by transmission electron microscopy. The particles were characterized by Fourier transform infrared, thermogravimetric analysis, and differential scanning calorimetry. Drug encapsulation efficiency, loading degree, and release profile were examined by high-performance liquid chromatography. Human breast cancer MDA-MB-231 was used to test the cytotoxicity. Flow cytometry and immunofluorescence imaging were used to study the PD-L1 inhibition in cell surface and exosomes. MDA-MB-231 and Jurkat co-culture studied T-cell activation and apoptosis.

Results: The particle size of the empty and drug-loaded micelles showed a size distribution with an average diameter of 54.62 ± 2.28 nm and 60.22 ± 2.56 nm, respectively. The encapsulation efficiency of BMS-T7 was 83.89 ± 5.59%. The release half-life of drug-loaded micelles was 48h. The IC_{50} of BMS-1166 was 28.77 μM in MDA-MB-231 cells. In addition, the BMS-T7 showed a better inhibitory effect on PD-L1 expression in breast cancer cells and exosomes than the naked drug. The formulation significantly restored T-cell function compared to the BMS-1166 treatment.

Conclusion: These results provide preliminary evidence indicating that BMS-T7 may have the potential to deliver drugs to breast cancer cells via active targeting and hold great promise in cancer immunotherapy drug delivery applications.

Keywords: PD-L1, BMS-1166, immunotherapy, breast cancer, micelles

Introduction

In the last decade, immune checkpoint blockade has emerged as a transformative approach in cancer therapy, offering new avenues to treat various malignancies, including breast cancer. Immune checkpoints are regulatory pathways in the immune system that maintain self-tolerance and prevent autoimmunity while minimizing damage to normal tissues during immune responses. While immune checkpoint blockade (ICB) therapy, particularly targeting the programmed cell death protein 1 (PD-1) and its ligand PD-L1 axis, has revolutionized treatment for certain breast cancer patients, its clinical application is not without significant challenges. A key issue is the relatively low overall response rate to ICB therapy, with benefits being confined to a select group of patients. This constraint underscores the pressing need to refine and enhance ICB therapy strategies.[1–4] PD-1 and PD-L1 are integral components of an immune checkpoint pathway that regulates immune responses.[5,6] These proteins are crucial in maintaining self-tolerance and preventing autoimmunity, but they are also exploited by tumors to evade immune surveillance. PD-1 is a 288-amino acid type I transmembrane protein belonging to

Received: 20 September 2024
Accepted: 28 December 2024
Published: 8 January 2025

the immunoglobulin superfamily. It contains an extracellular IgV-like domain, a transmembrane region, and an intracellular tail with immunoreceptor tyrosine-based inhibitory motifs and immunoreceptor tyrosine-based switch motifs.[7] PD-1 is primarily expressed in activated T cells, B cells, natural killer cells, dendritic cells, and monocytes. Its expression is upregulated upon activation of these immune cells.[8,9] PD-L1 is a 290-amino acid type I transmembrane protein with an extracellular domain containing IgV-like and IgC-like regions, a transmembrane domain, and a short cytoplasmic tail. PD-L1 is expressed in various cells, including T cells, B cells, dendritic cells, macrophages, endothelial cells, and non-hematopoietic cells.[10] Its expression can be induced by inflammatory cytokines, particularly interferon-gamma (IFN-γ).[11] PD-L1 primarily binds to PD-1, delivering inhibitory signals that reduce T-cell activity, promoting immune tolerance and preventing tissue damage during inflammation. Some breast tumors upregulate PD-L1 expression as a mechanism to evade immune surveillance. By engaging PD-1 on tumor-infiltrating lymphocytes, PD-L1 suppresses anti-tumor immune responses, allowing tumor cells to grow and proliferate unchecked.[12,13] When PD-L1 on tumor cells binds to PD-1 receptors on tumor-infiltrating lymphocytes, it inhibits the T cells' activity. This engagement transmits a co-inhibitory signal that reduces T cell proliferation, cytokine production, and cytotoxic activity. The binding of PD-1 to PD-L1 recruits phosphatases like SHP-2 to the intracellular domain of PD-1. These phosphatases dephosphorylate key signaling molecules involved in T-cell activation, such as CD3ζ and ZAP70.[14] This dephosphorylation effectively "turns off" the T cell, preventing it from attacking the tumor cell. In breast cancer, PD-L1 expression varies significantly among different subtypes. PD-L1 expression in breast cancer has been studied as a potential prognostic marker. Higher PD-L1 levels may correlate with better responses to certain therapies and possibly improved survival rates in some patient subsets.[15]

Triple-negative breast cancer (TNBC) often shows higher levels of PD-L1 expression compared to other breast cancer subtypes. This has been linked to the aggressive nature of TNBC and the ability to evade immune responses more effectively. TNBC has traditionally been considered poorly immunogenic, the combination of PD-1/PD-L1 inhibitors with chemotherapy has shown promising efficacy in both early and metastatic settings. The Food and Drug Administration (FDA) approved pembrolizumab combined with nab-paclitaxel as a first-line treatment for metastatic TNBC, following the successful outcomes of the KEYNOTE-355 study. Furthermore, the KEYNOTE-522 trial marked a significant advance with the FDA's approval of pembrolizumab in combination with chemotherapy for early-stage TNBC, demonstrating improved pathologic complete remission rates. These approvals have established a new standard of care for certain breast cancer patients and have spurred ongoing research to identify potential biomarkers for PD-1/PD-L1 therapy and to understand the mechanisms underlying treatment response.[16]

However, the response rate to PD-1/PD-L1 inhibition therapy in breast cancer patients is currently low, with only a subset of patients experiencing benefits. This is particularly evident in TNBC, where the clinical benefits of ICBs are inconsistent, with response rates ranging from 15 to 60%, whether used as monotherapy or in combination.[16] The variability in response is partly attributed to the complex and dynamic nature of the tumor microenvironment (TME), which influences breast cancer progression and treatment outcomes.[17] The efficacy of ICBs is closely linked to both the intrinsic properties of the tumor and the interactions within the TME.

Since the FDA approved the first immune checkpoint inhibitor in 2011, numerous therapies targeting the PD-1/PD-L1 axis have been developed. Anti-PD-1 antibodies include Pembrolizumab (Keytruda) and nivolumab (Opdivo),[18] and anti-PD-L1 antibodies include atezolizumab (Tecentriq), durvalumab (Imfinzi), and avelumab (Bavencio).[19] However, most of these therapies are based on therapeutic antibodies that, despite their efficacy, have limitations such as high production costs, potential for immunogenic reactions, and challenges in tumor penetration.[20] The molecular weight of monoclonal antibodies is generally about 150,000 daltons (150 kDa). In contrast, small molecule inhibitors are low molecular weight compounds. Due to their low molecular weight and small size, small molecules have unique pharmacokinetic properties, offering higher tissue permeability and tumor penetration efficiency than monoclonal antibodies. However, cell membranes are selectively permeable to most molecules, and small-molecule drugs typically enter cells through passive diffusion or active transport mechanisms to act on their targets. Moreover, small-molecule inhibitors offer a potential alternative due to their lower cost, higher stability, and better tumor penetration efficiency.[21] However, their development has been slow due to the difficulties in targeting the flat and hydrophobic surfaces of PD-1/PD-L1 interactions.[22]

BMS-1166 is a small-molecule PD-L1 inhibitor. By inhibiting PD-L1, BMS-1166 helps prevent the interaction between PD-L1 and PD-1, thereby promoting the activation of T cells and enhancing the immune response against cancer

cells.[23] These inhibitors block the immune checkpoint and alter the post-translational processing of PD-L1, leading to its misfolding and degradation. Such mechanisms suggest that small molecules could effectively restore immune system activity against tumor cells.[24,25]

The transferrin receptor 1 (TfR1), also known as cluster of differentiation 71, is a type II transmembrane glycoprotein that binds transferrin and plays a critical role in cellular iron uptake through the interaction with iron-bound Tf.[26–28] Iron is required for multiple cellular processes and is essential for DNA synthesis and, thus, cellular proliferation.[29,30] TfR1 exhibits a pronounced overexpression in breast cancer tissues, with a particularly striking increase observed in more aggressive subtypes such as TNBC. Furthermore, high TfR1 expression is closely associated with tumor proliferation, invasiveness, and poor prognosis in patients, making it a potential prognostic marker for breast cancer evaluation.[31] Due to its central role in cancer cell pathology, malignant cells often overexpress TfR1, and this increased expression can be associated with poor prognosis in different types of cancer. The elevated levels of TfR1 expression on malignant cells, its extracellular accessibility, its ability to internalize, and its central role in cancer cell pathology make this receptor an attractive target for antibody-mediated therapy.[32–34] TfR1 can be internalized through receptor-mediated endocytosis in anticancer drug conjugates, such as T7 (HAIYPRH) peptide.[35–37] Although TfR1 has been used extensively as a target for antibody-mediated cancer therapy over the years, interest continues to increase for both targeting the receptor for delivery purposes and its use as a direct anti-cancer agent.[26–28]

This study hypothesized that BMS-T7 (BMS-1166-loaded T7-modified poly (ethylene glycol)-poly(ε-caprolactone) (PEG-PCL) polymeric micelles) could inhibit PD-L1 expression, serving as a targeted immunotherapy for TfR1-positive breast cancer (Scheme 1). Through this innovative approach, this study combines the advantages of targeted delivery systems and small-molecule inhibitors to overcome the current challenges in cancer immunotherapy, paving the way for more effective and accessible treatments for breast cancer and other malignancies.

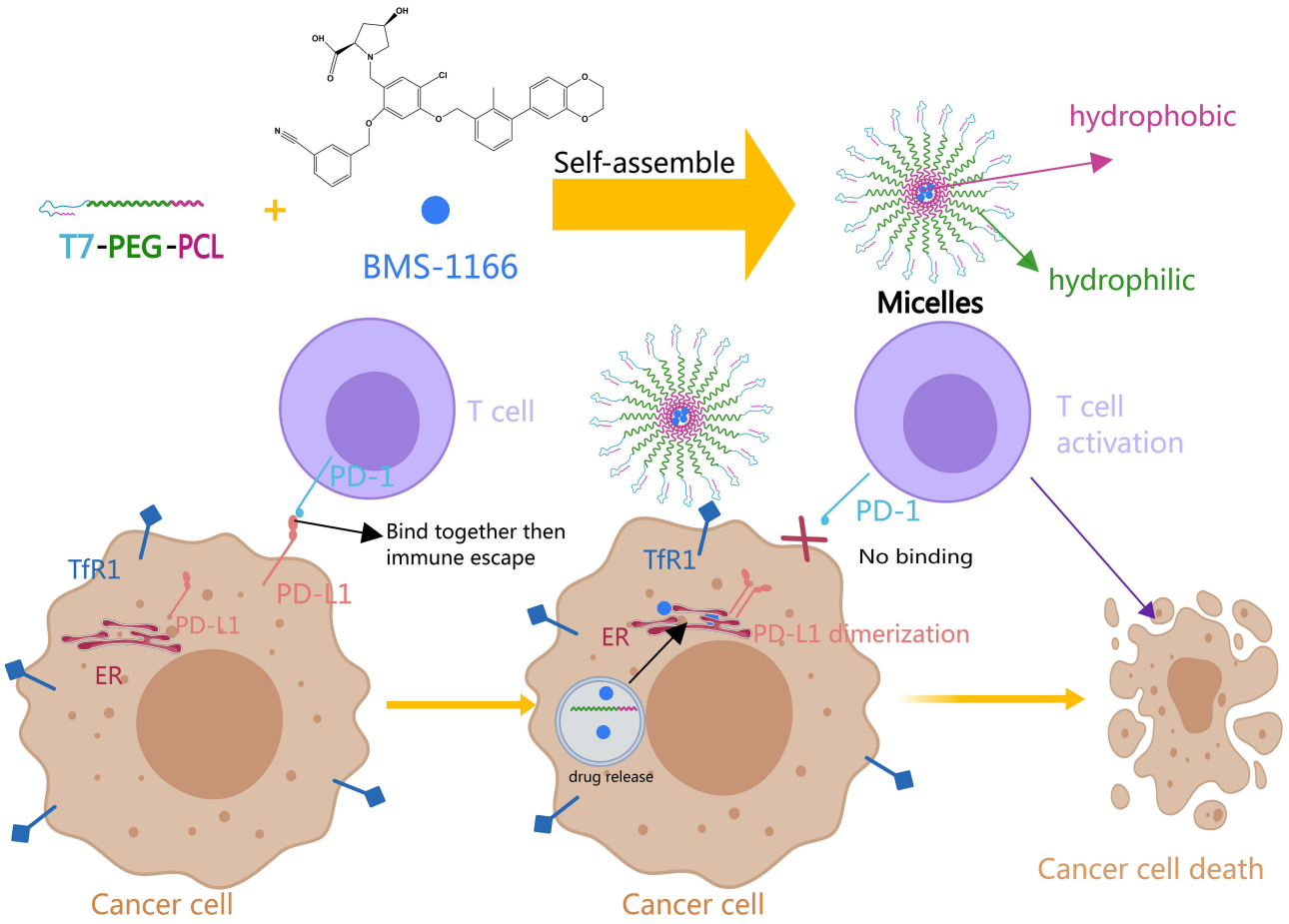

Scheme 1 Mechanism Diagram: targeted drug delivery micelles inhibit PD-1/PD-L1 axis in breast cancer. Created with MedPeer (www.medpeer.cn).

https://doi.org/10.2147/IJN.S497089

Materials and Methods

Materials

BMS-1166 was bought from Dongcang Biotechnology Co., Ltd. (Shanghai, China). The T7-PEG-PCL polymer (PEG molecular weight: 10,000 Da, PCL molecular weight: 5000 Da) was purchased from MELOPEG (Shanghai, China, Catalog Number: 401501). RPMI 1640 medium, fetal bovine serum and penicillin-streptomycin were purchased from Corning Inc. (Auckland, New Zealand) and Gibco, Thermo Fisher Scientific Inc. (Waltham, MA, USA), respectively. MDA-MB-231 human breast cancer and Jurkat cell line were purchased from the Peking Union Medical College Cell Culture Center (Beijing, China). Recombinant Alexa Fluor®488 Anti-PD-L1 antibody was purchased from Abcam Inc. (Cambridge, MA, USA). Human Interferon-gamma recombinant protein was purchased from Cell Signaling Technology, Inc. (Danvers, MA, USA).

Micelle Preparation

To prepare the BMS-T7, both T7-PEG-PCL polymer and BMS-1166 drug were initially dissolved in dimethylformamide (DMF) (Aladdin, Shanghai, China) at a mass ratio of 20:1. Following complete dissolution, the solution was transferred into a dialysis bag (Biovake, China) with a 7000 molecular weight cut-off to facilitate the removal of DMF. Dialysis was carried out in distilled water for a period ranging from 12 to 24 hours, with midway changes of water three times, to ensure thorough solvent removal, thereby forming the drug-loaded micelles.

Particle Size and Zeta Potential

After dialysis, the micelle solution was retrieved from the dialysis bag for analysis. Particle size and zeta potential measurements were performed at room temperature using dynamic light scattering (DLS) (Zetasizer Nano ZS ZEN3600). This technique provided rapid and accurate assessments of the micelles' hydrodynamic size and surface charge in solution.

Transmission Electron Microscopy

Ten microliters of the sample were pipetted and added onto the copper net for precipitation for 1 min. The floating liquid was removed by filter paper and dried at room temperature for several minutes. Ten microliters of uranyl acetate were dropped onto the copper mesh for precipitation for 1 min, and the floating liquid was absorbed by filter paper and dried at room temperature for several minutes. Electron microscopy analysis was conducted using a HITACHI HT7800 transmission electron microscope, with an acceleration voltage range of 80–120 kV, by Scientific Compass.

Fourier Transform Infrared Spectroscopy

Fourier Transform Infrared (FTIR) spectroscopy was conducted using a Thermo IS10 FTIR spectrometer. A quantity of 5 mg of the sample powder was precisely weighed and subjected to analysis. The spectral scan covered a range from 500 to 4000 cm^{-1}, capturing a comprehensive spectrum to identify various chemical bonds and functional groups in the sample.

Thermogravimetric Analysis

Thermogravimetric analysis (TGA) was performed using a PerkinElmer TGA 4000 thermal analyzer. The sample was analyzed under a continuous airflow to simulate oxidative conditions commonly encountered in practical environments. The temperature was progressively increased from 25°C to 800°C at a steady rate of 20°C per minute, allowing for the detailed observation of the material's thermal stability and decomposition characteristics.

Differential Scanning Calorimetry

Differential scanning calorimetry (DSC) analysis was conducted using a PerkinElmer DSC 8000 instrument. Measurements were performed under a controlled atmosphere, with airflow maintained throughout the experiment. The temperature range for the analysis was set from 25°C to 800°C. A uniform heating rate of 20°C per minute was applied to ensure consistent thermal conditions during the analysis.

Drug Encapsulation Efficiency, Loading Degree, and Release Profile

Encapsulation efficiency is the percentage of the initial drug encapsulated within the delivery system (eg, nanoparticles, micelles).

$$\mathrm{EE}\ (\%) = \left(\frac{\text{Mass of Encapsulated Drug}}{\text{Mass of Initial Drug}}\right) \times 100$$

Drug loading degree is the ratio of the amount of drug encapsulated to the total weight of the drug-loaded delivery system.

$$\mathrm{DLD}\ (\%) = \left(\frac{\text{Mass of Encapsulated Drug}}{\text{Mass of Drug Loaded Delivery System}}\right) \times 100$$

The encapsulation efficiency and drug loading degree of the BMS-T7 were quantitatively analyzed using Agilent1260 high-performance liquid chromatography (HPLC). Mobile phase A was deionized distilled H_2O, and B was methanol. The liquid chromatography column (EC-C18, 4.6 mm × 100 mm, Agilent) was equilibrated with 50% mobile phase A and then separated through the liquid chromatography column. The corresponding liquid gradient was set as 0–0.5 min, 50% A, 50% B, and 0.5–2 min, respectively. The linear gradient of A was 50–10%, the linear gradient of B was 50–90%, 2–5 min, and the linear gradient of A and B was 10%, 90%, 5–5.5 min, respectively, the linear gradient of A was 10–50%, the linear gradient of B was 90–50%, 5.5–8 min, and the linear gradient of A was 10–50%. Liquid A and B were 50%, respectively, with a 0.8 mL/min flow rate. The retention time was 4.3 min. This method facilitated precise measurement of the amount of BMS-1166 encapsulated relative to the total amount of drug used in the formulation process. Drug release profiles were also determined through HPLC by analyzing the concentration of BMS-1166 released from the micelles into the medium over time under phosphate-buffered saline solution at 37 °C.

Cytotoxicity

Cytotoxicity was assessed using the cell counting kit-8 (CCK-8, GLPBIO, USA). MDA-MB-231 cells were seeded in 96-well plates at a density of 5,000 cells per well in 100 μL of complete culture medium and allowed to adhere for 24 hours. After adhesion, the culture medium was removed, and cells were washed gently with phosphate-buffered saline (PBS). Subsequently, cells were treated with 100 μL of the prepared BMS-T7 solutions at various concentrations. MDA-MB-231 cells were incubated with the micelle solutions for 48 hours at 37°C in a 5% CO_2 atmosphere. At the end of each incubation period, 10 μL of CCK-8 reagent was added to each well, and the plates were incubated for an additional 2 hours at 37°C, protected from light. The absorbance was measured at 450 nm using a microplate reader (Thermo Fisher Scientific, USA). The cell viability was calculated as the percentage of absorbance relative to the untreated control wells.

Flow Cytometry

The effect of BMS-T7 on the expression of PD-L1 receptors was studied by Agilent NovoCyte 3000 flow cytometry. The MDA-MB-231 cells were seeded in 6-well plates overnight. Then, empty micelles, 10 μM of BMS-1166 and BMS-T7, containing 10 μM BMS-1166, were added respectively with 100 ng/mL INF-γ. After 48 h of treatment, the cells were collected. Later, the collected cells were incubated in PBS buffer, followed by the recombinant Alexa Fluor® FITC Anti-PD-L1 antibody (1/100 dilution) for 30 min at 4 °C for 30 minutes. Finally, the cells were washed and resuspended in PBS buffer at a density of 1×10^6 cells/mL for PD-L1 expression determination using flow cytometry.

Immunofluorescence Imaging

Immunofluorescence imaging examined the effect of BMS-T7 on the expression of PD-L1. The MDA-MB-231 cells were seeded overnight in a glass bottom cell culture dish (801002, NEST). Then, empty micelles, 10 μM of BMS-1166 and BMS-T7, containing 10 μM BMS-1166, were added respectively with 100 ng/mL INF-γ. After 48 h of treatment, the cells were fixed with 4% formaldehyde for 10 minutes, permeabilized with 0.1% Triton X-100 for 5 minutes, and then blocked with 1% BSA for 1h. The cells were then incubated overnight at 4°C with recombinant Alexa Fluor®488 Anti-PD-L1 antibody (1/100 dilution). One milliliter of DAPI staining solution was added and left at room temperature for

3–5 minutes. DAPI staining solution was removed by aspiration and washed 2–3 times with PBS. They were observed directly under the Zeiss LSM900 confocal fluorescence microscope.

T Cell Apoptosis

MDA-MB-231 cells were incubated with 100 μg/mL IFN – γ for 48 hours to stimulate PD-L1 expression. Jurkat cells were treated with 2 μg/mL phytohemagglutinin (PHA) and 100 ng/mL phorbol 12-myristate 13-acetate (PMA) for 48 hours to induce PD-1 expression. For PD-1 blockage, the cells were incubated with 10 μg/mL anti-PD-1 antibody (R380854, Zenbio, Chengdu, China) for 3 hours. Jurkat and MDA-MB-231 cells were mixed (1:10) and seeded in a 96-well plate to study the apoptosis induction. The cells were co-cultured for 24 hours, and then 100 μL of Caspase-Glo® 3/7 reagent (G8091, Promega) was added to each well. The plate was incubated at 37 °C for 1 hour, and luminescence was measured.

T Cell Activation

T cell activation was studied by Luc-Pair™ Firefly Luciferase HS Assay Kit (LF007, GeneCopoeia, Rockville, MD, USA). Jurkat cells were transfected with the interleukin (IL)-2 reporter plasmid pIL2-luc (Limibio Co., Ltd, Shanghai, China) using the TransIT-Jurkat transfection reagent (MIR 2120, Mirus Bio LL). Twenty-four hours post-transfection, the cells were treated with 2 μg/mL PHA and 100 ng/mL PMA for 48 hours to induce PD-1 expression. Jurkat and MDA-MB-231 cells were mixed at 1:10 and seeded in a 96-well plate. After 24 hours of incubation, Jurkat cells were harvested, and the luciferase activity driven by the IL-2 promoter was measured to assess T-cell activation.

Exosomes Extraction

Exosomes were removed from the serum by ultracentrifugation to prepare the exosome-depleted medium. FBS was centrifuged at 100,000 × g for 2 h at 4°C. After centrifugation, the supernatant was collected and filtered through a 0.22 μm filter membrane to remove residual particulate matter. After MDA-MB-231 cells were cultured to 80–90% confluence, the growth medium was replaced with an exosome-depleted medium. After 48 hours of incubation, the supernatant was collected and mixed with the Exosome Isolation Q3 kit (EIQ304001, Wayen Biotechnologies, Shanghai, China) at a volume ratio of 2:1 by gently turning the tube up and down to ensure even mixing. After an overnight incubation at 4 °C, the mixture was centrifuged at 3000 × g for 60 minutes at 4 °C. The pellet was resuspended in 1 mL supernatant and centrifuged at 10,000 × g for 10 minutes at 4 °C. The resulting pellet was resuspended in 100 μL PBS and centrifuged at 10,000 × g for 5 minutes at 4 °C. The resulting supernatant was a PBS suspension containing exosomes from the cell culture supernatant.

PD-L1 Expression on Exosomes

The diluted exosome samples were mixed with CD9 positive magnetic beads (10620D, Invitrogen, Carlsbad, CA, USA) and incubated overnight at 4 °C with gentle shaking. Recombinant Alexa Fluor® FITC Anti-PD-L1 antibody (1/100 dilution) was added to the exosome-magnetic bead mixture. The mixture was incubated for 1 hour at 4 °C with gentle shaking. The magnetic beads were washed three times with PBS. Magnetic beads were collected using a magnetic stand. The stained magnetic beads were resuspended in PBS and ready for flow cytometry analysis.

Statistical Analysis

GraphPad Prism 10 software was used for statistical analysis. The experimental results were expressed as mean ± standard deviation. A *t*-test was used to compare the means between the two groups. Data were analyzed by one-way analysis of variance (ANOVA), followed by Tukey's test for comparison between groups. In all comparisons, statistical significance was set at $p \leq 0.05$.

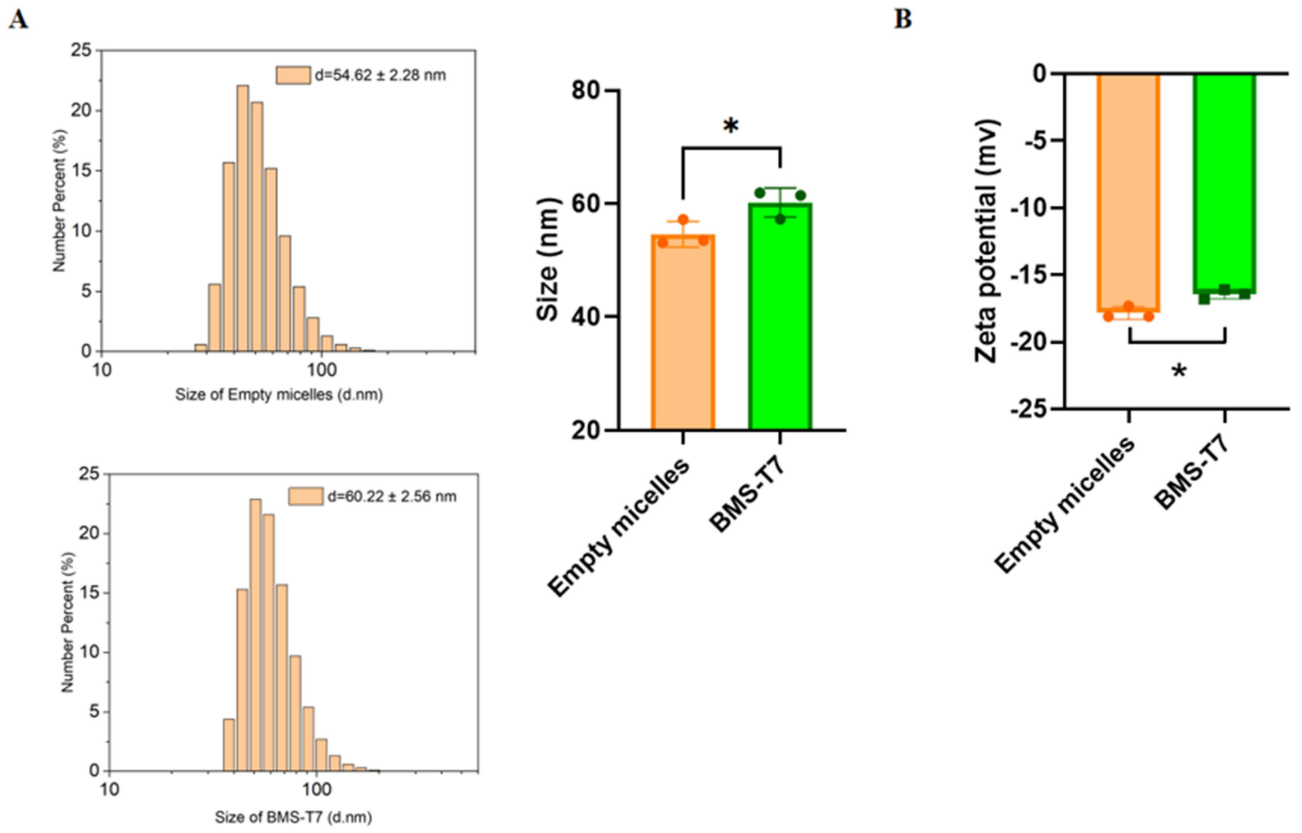

Figure 1 Characterization of empty micelle and BMS-T7. (**A**) Particle sizes and distributions. (**B**) Zeta potentials. (Mean ± SD, n = 3). (*: $p<0.05$).

Results

Particle Size and Zeta Potential of BMS-T7

The particle size of the empty micelles showed a size distribution with an average diameter of 54.62 ± 2.28 nm. The polydispersity indexes (PDIs) of the empty micelle and BMS-T7 were 0.171 ± 0.03 and 0.165 ± 0.06, respectively. The distribution indicated good uniformity in the particle size of the micelles. The BMS-T7 had a slightly larger diameter of

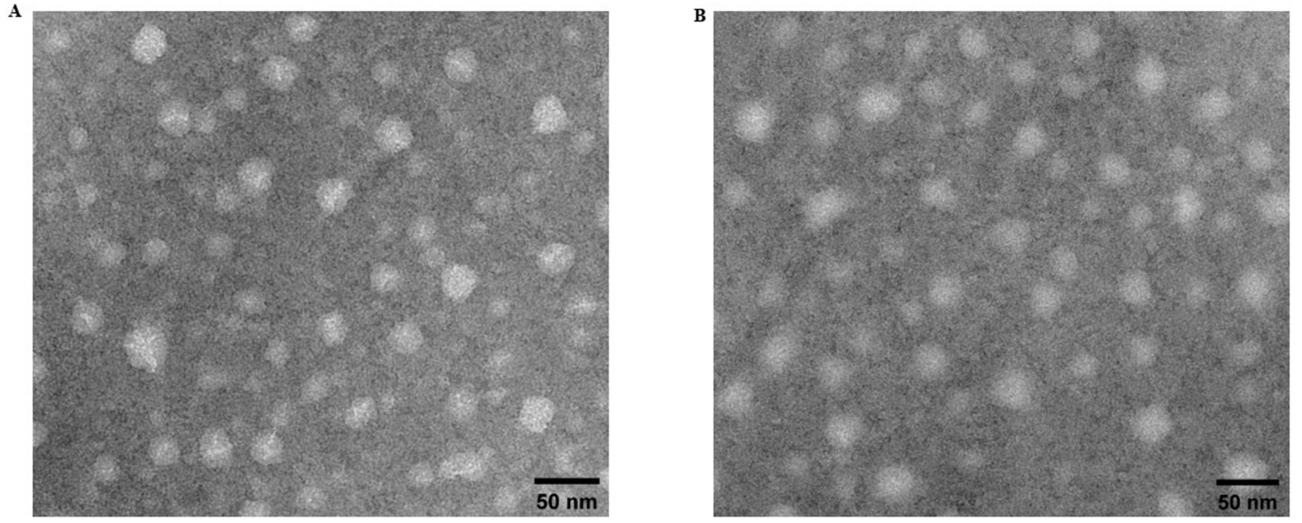

Figure 2 Transmission Electron Microscopy (TEM) Images: TEM images of (**A**) empty and (**B**) BMS-T7, showcasing their morphology.

https://doi.org/10.2147/IJN.S497089

60.22 ± 2.56 nm (Figure 1A). The increase in size could be attributed to the encapsulation of BMS-1166 within the micelles. The zeta potential of the empty micelles was slightly more negative than that of the BMS-T7. The empty micelles exhibited a zeta potential of −17.83 ± 0.46 mV, while the zeta potential of the BMS-T7 was −16.43 ± 0.35 mV (Figure 1B). The diameters of nanoparticles were measured using TEM image analysis software, Nano Measurer. A total of 100 particles were analyzed from TEM images. The particle sizes of the empty and BMS-T7 were 21.63 ± 0.84 nm (Figure 2A) and 23.58 ± 0.98 nm (Figure 2B), respectively, as determined by TEM.

Characterization of BMS-T7 by FTIR, TGA and DSC Analysis

FTIR (Figure 3), TGA (Figure 4) and DSC (Figure 5) analyses were conducted on BMS-T7, physical mixture, empty micelles, and BMS-1166 naked drug. In the BMS-1166 spectrum, the broad peak around 3200–3400 cm^{-1} indicates O-H stretching, characteristic of hydroxyl groups. The 2800–3000 cm^{-1} peaks suggest C-H stretching vibrations from alky chains. The peaks at 2200–2250 cm^{-1} indicate the presence of a nitrile group (C≡N). The empty micelles spectrum is similar to general polymer spectra with peaks related to C-H stretching, C=O stretching in esters, and ether linkages. In the physical mixture spectrum, it showed combined features of both empty micelles and BMS-1166. In the BMS-T7 spectrum, the nitrile peak (2200–2250 cm^{-1}) was less prominent or shifted, suggesting encapsulation rather than simple physical mixing. The TGA of BMS-1166 exhibited a clear, single-stage degradation pattern, simplifying drug decomposition identification. The TGA of empty micelles showed thermal stability up to a higher temperature than BMS-1166, followed by a steady degradation. The TGA of the physical mixture displayed a weight loss pattern that started earlier than the empty micelles, suggesting the presence of other degradable components along with the carrier material. The degradation profile of BMS-T7 suggested a more complex decomposition than the empty micelles, likely due to the drug's and carrier system's combined stability characteristics.

The thermal transitions of the physical mixture mostly followed the empty micelles profile but with some minor peaks, likely from the drug. The reduced intensity and shift of transition peaks of the BMS-T7 compared to BMS-1166

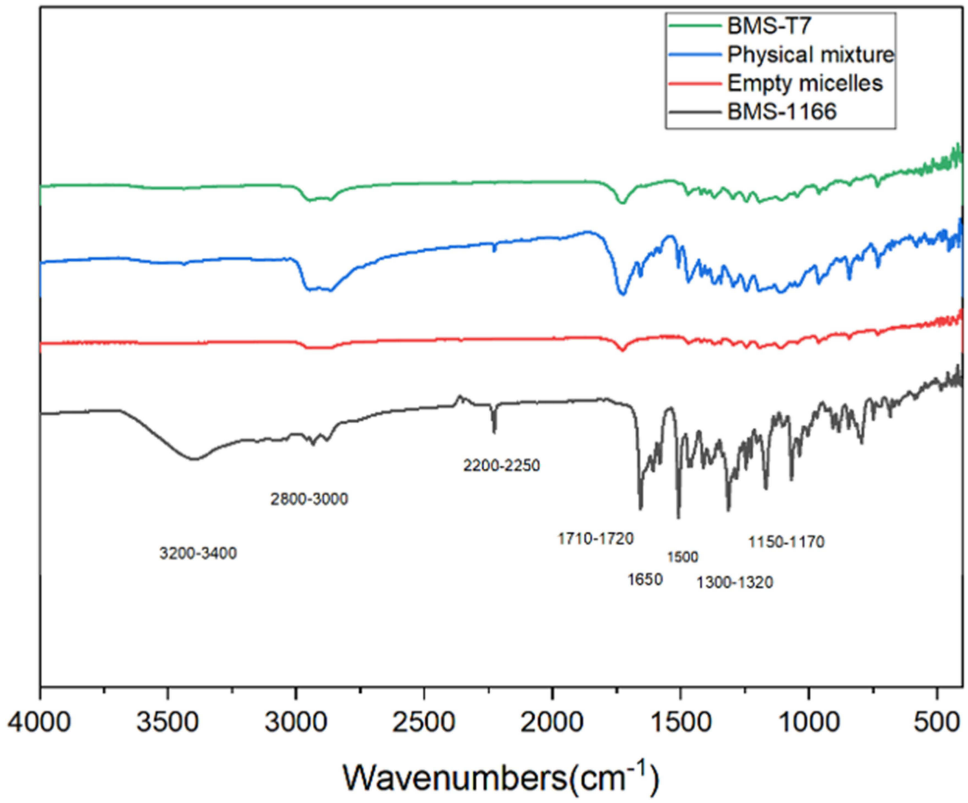

Figure 3 Fourier transform infrared (FTIR) spectroscopy analysis of BMS-T7, physical mixture, empty micelles, and BMS-1166.

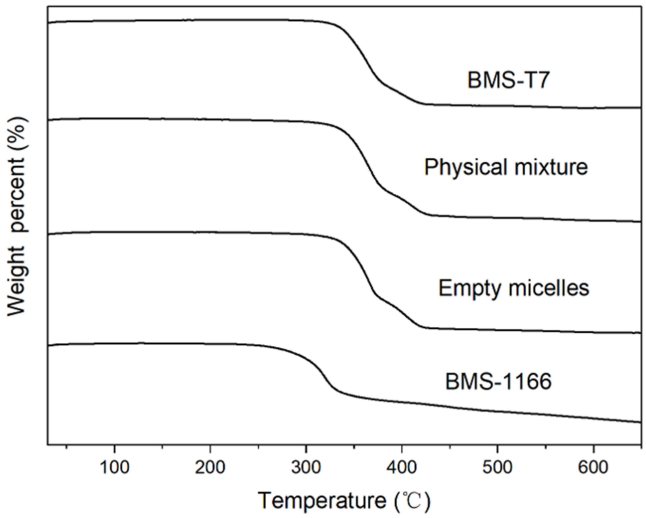

Figure 4 Thermogravimetric analyses (TGA) of BMS-T7, physical mixture, empty micelle, and BMS-1166.

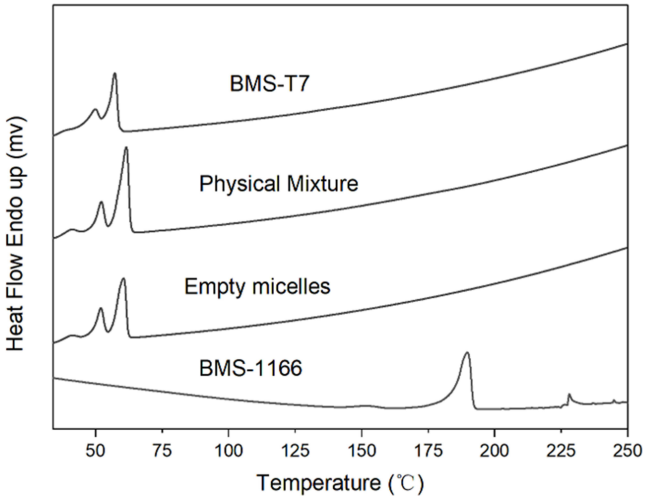

Figure 5 Differential scanning calorimeter (DSC) analysis of BMS-T7, physical mixture, empty micelle, and BMS-1166.

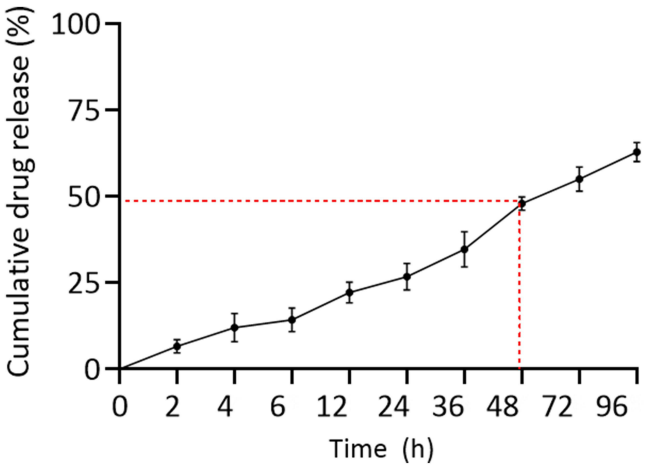

Figure 6 Drug Release Profile: Profile of BMS-1166 released from BMS-T7 over time. (Mean ± SD, n=3).

https://doi.org/10.2147/IJN.S497089

suggested that the drug was well-dispersed within the micelles, potentially in an amorphous state or interacting with the micelles' matrix.

Encapsulation Efficiency, Drug Loading Degree and Drug Release of BMS-T7

The drug loading degree of 4.95 ± 0.79% indicated the percentage of the total weight of the micelle comprised of the drug BMS-1166. The encapsulation efficiency was 83.89 ± 5.59%. Figure 6 shows a sustained release profile of BMS-1166 from the micelles. The release half-life of BMS-1166 from the micelle was around 48 h.

The IC_{50}s of BMS-1166 and BMS-T7

The IC_{50}s of BMS-1166 and BMS-T7 were 23.014 μM and 28.77 μM respectively. The 10 μM BMS-1166 naked drug and BMS-T7 did not show significant toxicities on MDA-MB-231 cells.

BMS-1166 Micelles Inhibited PD-L1 Expression

The expression of PD-L1 in MDA-MB-231 cells was ascertained through flow cytometry (Figure 7A) and immunofluorescence staining (Figure 7B). Subsequent statistical analysis was conducted on the flow cytometry data (Figure 7C) and the fluorescence intensity measurements from the immunofluorescence staining (Figure 7D). The results indicated that INF-γ could induce PD-L1 expression in MDA-MB-231 cells. However, empty micelle treatment did not alter PD-L1 expression compared to the control group, suggesting that the drug delivery carrier could not affect PD-L1 expression. In addition, the treatment with 10 μM BMS-1166 naked drug or loaded micelles could reduce PD-L1 expression significantly compared to INF-γ stimulated cells. Moreover, the BMS-T7 showed a better inhibitory effect on PD-L1 inhibition than the naked drug. The immunofluorescence staining results were consistent with flow cytometry.

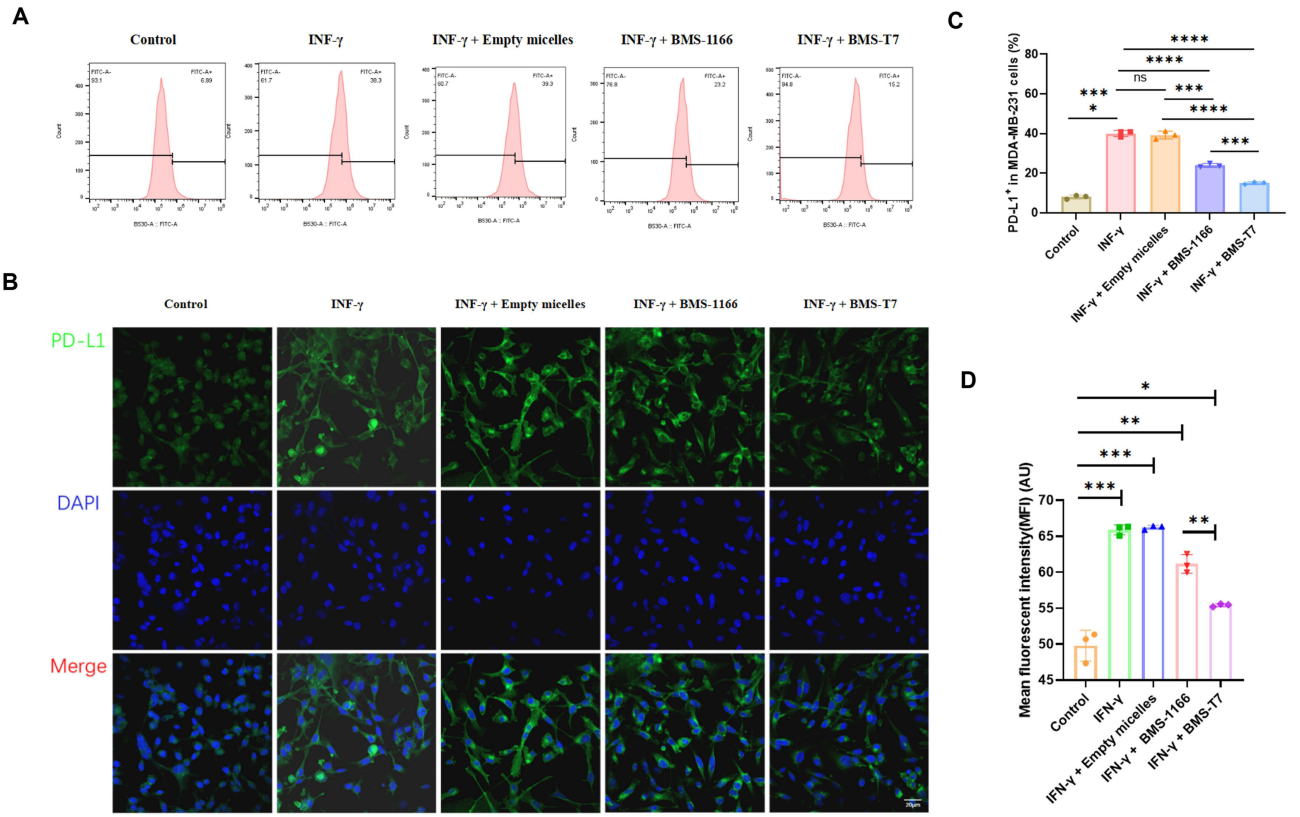

Figure 7 PD-L1 Expression in MDA-MB-231 Cells: (**A**) Flow cytometry and (**B**) immunofluorescence staining were used to determine PD-L1 expression. Statistical analysis of (**C**) flow cytometry and (**D**) fluorescence intensity measurements in immunofluorescence staining were performed. The white horizontal line in the figure represents the scale bar, which is 20 μm in length. (mean ± SD, n = 3) (ns: not significant, *: p<0.05, **: p<0.01, ***: p<0.001, ****: p<0.0001).

 https://doi.org/10.2147/IJN.S497089

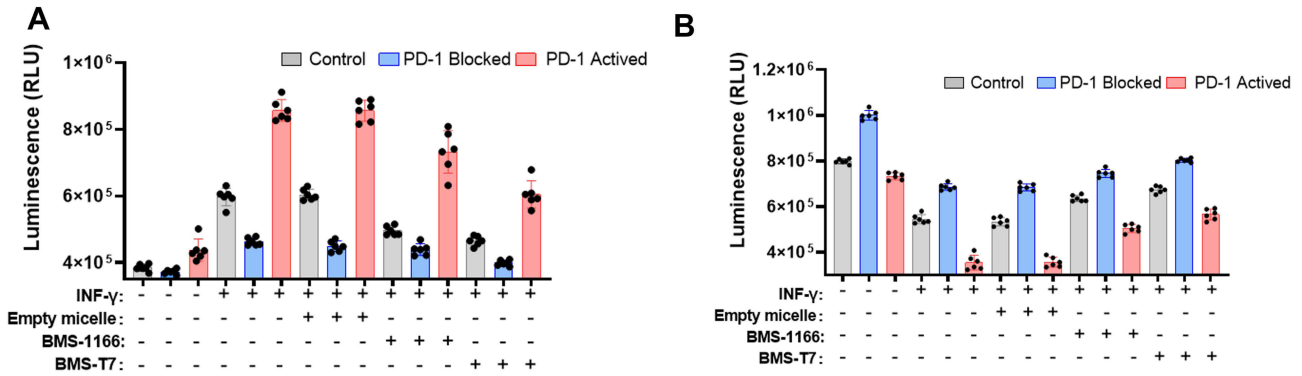

Figure 8 T Cell Function Restoration by BMS-T7. Assessment of apoptosis induction (**A**) and IL-2-luciferase expression (**B**) in Jurkat cells co-cultured with MDA-MB-231 cells. IFN – γ was used to induce PD-L1 expression on MDA-MB-231 cells. The PD-1 expression on Jurkat cells was either blocked by anti-PD-1 antibody or activated by PHA and PMA. (Mean ± SD, n = 6).

BMS-T7 Restored T Cell Function

Jurkat cells were co-cultured with MDA-MB-231 cells to study the restoration effect of BMS-T7 on T-cell function. Figure 8A showed that T-cell apoptosis was significantly induced by co-culturing with IFN-γ-stimulated MDA-MB-231 cells. This suggested that the upregulation of PD-L1 on MDA-MB-231 cells enhanced its immune evasion against T cells. On the other hand, T-cell apoptosis could be attenuated by BMS-1166 treatment, which indicated effective blockage of the PD-1/PD-L1 interaction. In addition, the micelle formulation further reduced the apoptosis reduction in T cells.

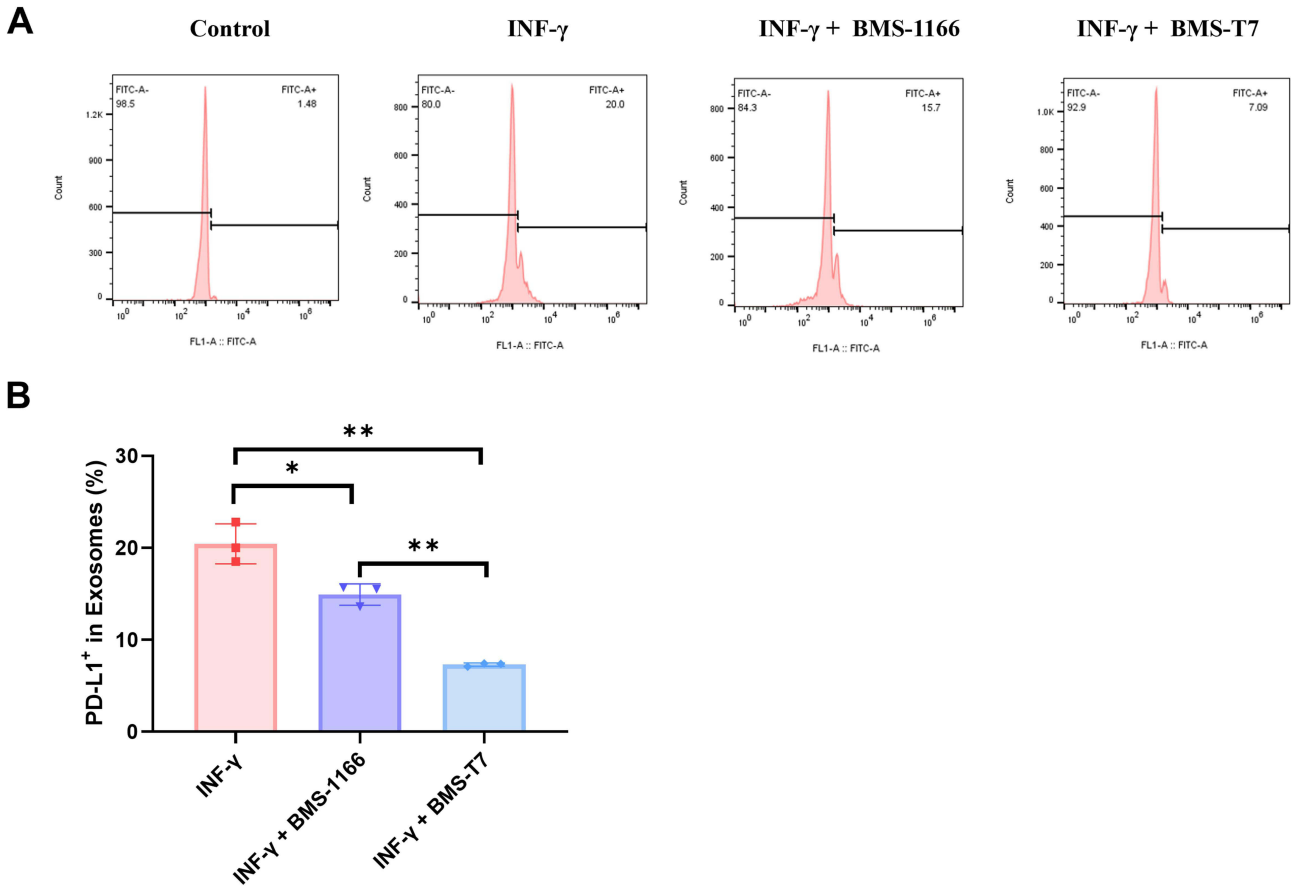

Figure 9 PD-L1 Expression on Exosomes: Representative results of PD-L1 expression on exosomes determined by (**A**) flow cytometry and (**B**) statistical analysis of the positive rate. (Mean ± SD; n = 3; *: p<0.05, **: p<0.01) (**B**).

https://doi.org/10.2147/IJN.S497089

The T cell activation bioassay results in Figure 8B demonstrated that IFN-γ treatment of MDA-MB-231 cells significantly reduced IL-2 promoter-driven luciferase activity in co-cultured Jurkat T cells, indicating suppressed T cell activation due to increased PD-L1 expression. However, treatment with BMS-1166, particularly the micelle formulation, effectively restored T cell activity, as evidenced by increased luciferase activity. These findings highlighted the potential of BMS-T7 to counteract PD-L1 positive tumor-induced T-cell suppression.

BMS-T7 Suppressed PD-L1 Expression in Exosomes

The expression of PD-L1 in exosomes was quantified by flow cytometry. Figure 9 revealed that INF-γ could also increase PD-L1 expression in breast cancer exosomes compared to the control group. When cells were treated with BMS-1166, the expressions of PD-L1 were significantly reduced. In addition, the inhibitory effect of BMS-1166 was enhanced by the micelle formulation.

Discussion

This study explored the efficacy of BMS-T7 as a targeted therapeutic approach in PD-L1 inhibition for breast cancer immunotherapy. The experimental data underline several critical aspects of micelle-mediated drug delivery systems, showcasing the potential of this technology in enhancing the bioavailability and efficacy of immunotherapeutic agents.

The small increase in size upon drug loading suggested the successful incorporation of BMS-1166 into the micelles without significantly disrupting their structure. The increase in particle size after drug encapsulation in micelles observed in our study aligns with previous research.[38,39] The narrow size distribution in both cases indicated a well-controlled micelles formation process, which is crucial for ensuring consistent drug delivery and biodistribution.

Zeta potential is a critical parameter for understanding the stability of colloidal dispersions. Higher absolute values (positive or negative) typically indicate better stability due to electrostatic repulsion preventing aggregation. Compared with empty micelles, the zeta potential of BMS-T7 was significantly reduced, indicating that the drug was successfully incorporated into the micelle. The micelles retained good stability even after drug loading, making them potentially effective for drug delivery.

The TEM images showed that empty and BMS-T7 were well-dispersed with no significant aggregation. The uniform and discrete appearance of the micelles in the TEM images further confirmed their stability and successful formulation. This uniformity was crucial for achieving predictable in vivo behavior and efficient targeting of the cancer cells. Our observations that the particle size measured by TEM is smaller than that measured by DLS are consistent with previous studies. Wang et al attribute this difference to the fact that DLS measures the hydrodynamic diameter, including the solvent layer. In contrast, TEM provides a more accurate measurement of the core particle size.[40]

The FTIR analysis of the physical mixture exhibited overlapping features from BMS-1166 and other components, confirming the presence of drug and carrier materials without chemical interaction. The FTIR of empty micelles lacks the characteristic peaks of BMS-1166, showing mainly the carrier material's peaks. The FTIR analysis of BMS-T7 showed diminished characteristic drug peaks, suggesting encapsulation, which may mask or shift these peaks due to interactions or environmental changes within the structure of the micelles.[41]

The TGA results demonstrated that the BMS-T7 possess distinct thermal properties compared to both the drug and the empty micelles, indicating the influence of drug encapsulation on the thermal stability of the system. The thermal transitions of BMS-1166 showed specific melting or transition peaks, indicative of its crystalline nature. The thermal transitions of empty micelles lacked significant peaks, which might indicate an amorphous or stable matrix at the tested temperature range.[41] The DSC analysis supported that the BMS-1166 was molecularly dispersed within the micelles, potentially altering its crystalline properties and stabilizing it in a non-crystalline form. Thermogravimetric analysis (TGA) and differential scanning calorimetry (DSC) results suggest that the micelles provide a stable environment for the drug, potentially protecting it from thermal and chemical degradation. This stability is crucial for maintaining the drug's functional integrity until it reaches its target.

The drug loading degree of 4.95 ± 0.79% indicated the percentage of the total weight of the micelle comprised of the drug BMS-1166. While this value was relatively low, it was typical for polymeric micelles, where high loading capacities could be challenging due to the physical and chemical properties of the drug and polymer. The high encapsulation

efficiency (83.89%) demonstrates the micelle's capability to load significant amounts of BMS-1166, minimizing potential drug wastage and enhancing therapeutic delivery to the target site. Our findings of low drug loading and high encapsulation efficiency in micelles are consistent with previous studies.[42] Aliabadi and Lavasanifar highlighted that the core-shell structure of micelles allows for high encapsulation efficiency by effectively trapping hydrophobic drugs despite the limited core volume, resulting in low overall drug loading.[42] The release half-life of BMS-1166 from the micelle was around 48 h. Our micelles' half-release time of 48 hours is consistent with previously reported data.[39] Kedar et al indicated that micelles intended for sustained drug delivery generally exhibit half-release times between 24 and 72 hours, contingent upon the drug and micelle formulation.[39] The release profile suggested that this formulation could deliver the drug in a sustained and controlled manner. The sustained release profile was desirable for therapeutic applications, especially in cancer treatment, where maintaining a consistent drug concentration can enhance therapeutic efficacy and minimize side effects. The controlled release profile further supports the use of these micelles in sustained drug delivery applications, which is crucial for maintaining therapeutic drug levels in tumor environments.

The flow cytometry and immunofluorescence staining results illustrate that free BMS-1166 and its micelle-encapsulated form effectively inhibit the expression of PD-L1 in INF-γ stimulated MDA-MB-231 breast cancer cells. Notably, the micelle formulation enhances this effect, which could be attributed to improved cellular uptake and sustained release, thereby allowing for prolonged drug action at the target site. These findings hold significant implications for the clinical application of micelle technology in cancer therapy. The ability of the T7-PEG-PCL micelles to target TfR1 overexpressing breast cancer cells, coupled with their capability to deliver and release PD-L1 inhibitors like BMS-1166 effectively, highlights their potential as a promising tool in the arsenal against cancer. It aligns with the growing need for targeted therapies to provide higher efficacy at lower doses, reducing potential side effects and improving patient compliance.

The increased apoptosis induction of Jurkat cells co-cultured with PD-L1-positive breast cancer cells demonstrated the role of PD-L1 in promoting the immune escape of the cells. However, BMS-1166 significantly reduces T cell apoptosis, confirming its potential to block PD-1/PD-L1 interaction and restore T cell function. Meanwhile, the targeted micelle formulation enhanced the efficacy of the encapsulated drug. This delivery strategy provides a promising avenue for improving cancer immunotherapy outcomes by ensuring sustained and targeted drug release. The ability to reduce T cell apoptosis via PD-L1 inhibition may suggest a potential strategy to enhance anti-tumor immunity. These findings have significant implications for the development of more effective cancer immunotherapies.

The study presents compelling evidence for the role of PD-L1 in mediating immune evasion, as shown by the suppression of T-cell activation by PD-L1-positive breast cancer cells. IFN-γ treatment upregulates PD-L1 expression on tumor cells, interacting with PD-1 on T cells, leading to decreased IL-2 production and reduced T cell activation. This mechanism underlines the tumor's ability to evade immune surveillance by impairing T-cell function. The introduction of BMS-1166, an immune checkpoint inhibitor, disrupts the PD-1/PD-L1 interaction, thereby restoring T cell activation. The significant increase in luciferase activity in the BMS-1166-treated groups supports this observation. Meanwhile, the micelle formulation of BMS-1166 demonstrates a more pronounced effect, suggesting enhanced delivery and efficacy. These results have significant implications for cancer immunotherapy. Revering T cell suppression through PD-L1 inhibition can enhance the anti-tumor immune response, providing a promising strategy for improving therapeutic outcomes.

Research on exosomal PD-L1 has gained significant attention in recent years due to its role in tumor immune evasion. Exosomes are small extracellular vesicles that facilitate intercellular communication, and PD-L1 carried on exosomes can inhibit T-cell function, thereby promoting tumor progression and resistance to immunotherapy. Recent research emphasizes that targeting exosomal PD-L1 could offer a novel therapeutic strategy, potentially overcoming resistance to PD-1/PD-L1 blockade therapies.[43] Moreover, exosomal PD-L1 could serve as a biomarker for predicting and monitoring treatment responses in cancer patients, including those with breast cancer.[44] The ongoing exploration of exosomal PD-L1 is likely to contribute to developing more effective and personalized cancer immunotherapies, addressing the limitations of current treatments.

BMS-1166 exhibits a unique mechanism of action by interfering with the glycosylation and maturation of PD-L1, ultimately preventing its export from the endoplasmic reticulum (ER) to the Golgi apparatus. This blockade results in the accumulation of under-glycosylated PD-L1 within the ER, effectively reducing its surface expression and subsequent secretion in exosomes.[45] The data shown in Figure 9 aligns with this mechanistic insight. The flow cytometry analysis (Figure 9A) reveals that treatment with BMS-1166, particularly when delivered through micelles, significantly decreases

 https://doi.org/10.2147/IJN.S497089

the percentage of PD-L1 expression in exosomes compared to the INF-γ treated group. This observation is supported by the statistical analysis in Figure 9B, where a notable reduction in PD-L1 expression in exosomes is evident in the BMS-1166 treated groups. These findings suggest that by trapping PD-L1 within the ER and preventing its maturation and transport, BMS-1166 diminishes the levels of PD-L1 available for incorporation into exosomes. Consequently, this inhibition of exosomal PD-L1 could reduce the immunosuppressive microenvironment often promoted by tumors, thereby enhancing the immune response against cancer cells. This mechanism highlights BMS-1166's potential as a therapeutic agent in overcoming resistance to immune checkpoint blockade therapies.

One of the primary limitations of this study is the specificity of BMS-1166, which is a small molecule inhibitor specific to human PD-L1 (hPD-L1) and does not interact with mouse PD-L1 (mPD-L1).[46] This specificity restricts the ability to conduct in vivo experiments using murine models, as BMS-1166 will not bind to PD-L1 in these species, thus limiting our ability to assess the drug's efficacy in *vivo* accurately. Consequently, our study has focused on in vitro experiments to verify the mechanism of action and initial efficacy of BMS-1166. Additionally, exploring the potential of co-delivering other immunomodulatory agents through these micelles could offer insights into synergistic therapeutic strategies, potentially broadening the scope of micelle applications in oncological therapies.

Conclusions

Our study successfully encapsulated BMS-1166 within T7-PEG-PCL micelles, demonstrating that this nanoformulation can be a promising candidate for targeted immunotherapy in breast cancer treatment. The drug-loaded micelles exhibited favorable stability, uniformity in particle size distribution, and a sustained drug release profile, which are essential characteristics for further in vivo investigation of their therapeutic efficacy and safety. The complementary analyses using Fourier-transform infrared spectroscopy (FTIR), thermogravimetric analysis (TGA), and differential scanning calorimetry (DSC) confirmed the successful encapsulation of BMS-1166 within the micelles, with observed changes in chemical, thermal, and physical properties indicating the integration of the drug within the micelles matrix.

In vitro experiments using breast cancer cell line models revealed that BMS-T7 has a superior inhibitory effect on PD-L1 expression compared to the free drug, both on the cell surface and in exosomes. This enhanced efficacy suggests that BMS-T7 may offer a more targeted approach to immunotherapy by specifically modulating PD-L1 expression in breast cancer cells.

While these findings are promising, we acknowledge the limitations of our study. The specificity of BMS-1166 for human PD-L1 restricts its application in murine models, which has implications for our ability to conduct in vivo studies. Additionally, the current work is confined to in vitro evaluations, and thus, the pharmacokinetics, biodistribution, and full therapeutic potential of BMS-T7 micelles in vivo remain to be elucidated. Future studies will address these limitations, including the development of alternative model systems or the design of new experiments that can accommodate the specificity of BMS-1166 to human PD-L1.

In conclusion, our work presents a novel nanoformulation, BMS-T7, demonstrating potential as a targeted PD-L1 inhibitor for breast cancer immunotherapy. The successful encapsulation and enhanced inhibitory effects on PD-L1 expression support the further development of this micelle system. However, the need for in vivo validation and the exploration of the micelles' behavior in biologicallyrelevant mediums are recognized as critical next steps in advancing this research.

Funding

This work was financially supported by the General Program of Zhejiang Provincial Natural Science Foundation (ZCLTGY24C1001), Wenzhou Association for Science and Technology (KJFW0219), and Wenzhou-Kean University 2022 International Collaborative Research Program (ICRP202201).

Disclosure

The authors report no conflicts of interest in this work.

References

1. Ferlay J, Soerjomataram I, Dikshit R, et al. Cancer incidence and mortality worldwide: sources, methods and major patterns in globocan 2012. *Int J Cancer*. 2015;136:E359–386. doi:10.1002/ijc.29210

2. Pardoll DM. The blockade of immune checkpoints in cancer immunotherapy. *Nat Rev Cancer*. 2012;12:252–264. doi:10.1038/nrc3239
3. Topalian SL, Drake CG, Pardoll DM. Immune checkpoint blockade: a common denominator approach to cancer therapy. *Cancer Cell*. 2015;27:450–461. doi:10.1016/j.ccell.2015.03.001
4. Emens LA. Breast cancer immunotherapy: facts and hopes. *Clin Cancer Res*. 2018;24:511–520. doi:10.1158/1078-0432.Ccr-16-3001
5. Xu W, Wu L, Xu M, Luo J, Chen G. Ethanol exposure up-regulates Pd-L1/Pd-1 immune checkpoint pathway and promotes mammary tumor development. *Front Oncol*. 2022;12:874156. doi:10.3389/fonc.2022.874156
6. Murata T. Human herpesvirus and the immune checkpoint Pd-1/Pd-L1 pathway: disorders and strategies for survival. *Microorganisms*. 2021;9:778. doi:10.3390/microorganisms9040778
7. Zak KM, Grudnik P, Magiera K, Dömling A, Dubin G, Holak TA. Structural biology of the immune checkpoint receptor Pd-1 and its ligands Pd-L1/Pd-L2. *Structure*. 2017;25:1163–1174. doi:10.1016/j.str.2017.06.011
8. Riella LV, Paterson AM, Sharpe AH, Chandraker A. Role of the Pd-1 pathway in the immune response. *Am J Transplant*. 2012;12:2575–2587. doi:10.1111/j.1600-6143.2012.04224.x
9. Wherry EJ. T cell exhaustion. *Nat Immunol*. 2011;12:492–499. doi:10.1038/ni.2035
10. Sun C, Mezzadra R, Schumacher TN. Regulation and function of the Pd-L1 checkpoint. *Immunity*. 2018;48:434–452. doi:10.1016/j.immuni.2018.03.014
11. Chen J, Feng Y, Lu L, et al. Interferon-Γ-induced Pd-L1 surface expression on human oral squamous carcinoma via Pkd2 signal pathway. *Immunobiology*. 2012;217:385–393. doi:10.1016/j.imbio.2011.10.016
12. Yamaguchi H, Hsu JM, Yang WH, Hung MC. Mechanisms regulating Pd-L1 expression in cancers and associated opportunities for novel small-molecule therapeutics. *Nat Rev Clin Oncol*. 2022;19:287–305. doi:10.1038/s41571-022-00601-9
13. Lin X, Kang K, Chen P, et al. Regulatory mechanisms of Pd-1/Pd-L1 in cancers. *Mol Cancer*. 2024;23:108. doi:10.1186/s12943-024-02023-w
14. Elfoly M, Mirza JY, Alaiya A, et al. Pd-L1 intrinsically promotes the proliferation of breast cancer cells through the Skp2-P27/P21 axis. *Can Cell Inter*. 2024;24:161. doi:10.1186/s12935-024-03354-w
15. Oner G, Önder S, Karatay H, et al. Clinical impact of Pd-L1 Expression in triple-negative breast cancer patients with residual tumor burden after neoadjuvant chemotherapy. *World J Surg Oncol*. 2021;19:264. doi:10.1186/s12957-021-02361-9
16. Jin M, Fang J, Peng J, et al. Pd-1/Pd-L1 immune checkpoint blockade in breast cancer: research insights and sensitization strategies. *Mol Cancer*. 2024;23:266. doi:10.1186/s12943-024-02176-8
17. Wang Q, Shao X, Zhang Y, et al. Role of tumor microenvironment in cancer progression and therapeutic strategy. *Cancer Med*. 2023;12:11149–11165. doi:10.1002/cam4.5698
18. Malmberg R, Zietse M, Dumoulin DW, et al. Alternative dosing strategies for immune checkpoint inhibitors to improve cost-effectiveness: a special focus on nivolumab and pembrolizumab. *Lancet Oncol*. 2022;23:e552–e561. doi:10.1016/s1470-2045(22)00554-x
19. Bhardwaj M, Chiu MN, Pilkhwal Sah S. Adverse cutaneous toxicities by Pd-1/Pd-L1 immune checkpoint inhibitors: pathogenesis, treatment, and surveillance. *Cutaneous Ocul Toxicol*. 2022;41:73–90. doi:10.1080/15569527.2022.2034842
20. Buchbinder EI, Desai A. Ctla-4 and Pd-1 pathways: similarities, differences, and implications of their inhibition. *Am J Clin Oncol*. 2016;39:98–106. doi:10.1097/coc.0000000000000239
21. Zhan MM, Hu XQ, Liu XX, Ruan BF, Xu J, Liao C. From monoclonal antibodies to small molecules: the development of inhibitors targeting the Pd-1/Pd-L1 pathway. *Drug Discov Today*. 2016;21:1027–1036. doi:10.1016/j.drudis.2016.04.011
22. Zarganes-Tzitzikas T, Konstantinidou M, Gao Y, et al. Inhibitors of programmed cell death 1 (Pd-1): a patent review (2010–2015). *Expert Opin Ther Patents*. 2016;26:973–977. doi:10.1080/13543776.2016.1206527
23. Zak KM, Grudnik P, Guzik K, et al. Structural basis for small molecule targeting of the programmed death ligand 1 (Pd-L1). *Oncotarget*. 2016;7:30323–30335. doi:10.18632/oncotarget.8730
24. Mao D, Xu M, Jiang Q, et al. A single nucleotide mixture enhances the antitumor activity of molecular-targeted drugs against hepatocellular carcinoma. *Front Pharmacol*. 2022;13:951831. doi:10.3389/fphar.2022.951831
25. Guzik K, Zak KM, Grudnik P, et al. Small-molecule inhibitors of the programmed cell death-1/programmed death-ligand 1 (Pd-1/Pd-L1) interaction via transiently induced protein states and dimerization of Pd-L1. *J Med Chem*. 2017;60:5857–5867. doi:10.1021/acs.jmedchem.7b00293
26. Laskey J, Webb I, Schulman HM, Ponka P. Evidence that transferrin supports cell proliferation by supplying iron for DNA synthesis. *Exp Cell Res*. 1988;176:87–95. doi:10.1016/0014-4827(88)90123-1
27. Torti SV, Torti FM. Iron: the cancer connection. *Mol Aspect Med*. 2020;75:100860. doi:10.1016/j.mam.2020.100860
28. Zhang C. Essential functions of iron-requiring proteins in DNA replication, repair and cell cycle control. *Protein and Cell*. 2014;5:750–760. doi:10.1007/s13238-014-0083-7
29. Tanaka H, Arakawa H, Yamaguchi T, et al. A ribonucleotide reductase gene involved in a P53-dependent cell-cycle checkpoint for DNA damage. *Nature*. 2000;404:42–49. doi:10.1038/35003506
30. Fraser ST, Midwinter RG, Berger BS, Stocker R. Heme oxygenase-1: a critical link between iron metabolism, erythropoiesis, and development. *Adv Hematol*. 2011;2011:473709. doi:10.1155/2011/473709
31. Habashy HO, Powe DG, Staka CM, et al. Transferrin receptor (Cd71) is a marker of poor prognosis in breast cancer and can predict response to tamoxifen. *Breast Cancer Res Treat*. 2010;119:283–293. doi:10.1007/s10549-009-0345-x
32. Richardson DR, Lane DJ, Becker EM, et al. Mitochondrial iron trafficking and the integration of iron metabolism between the mitochondrion and cytosol. *Proc Natl Acad Sci USA*. 2010;107:10775–10782. doi:10.1073/pnas.0912925107
33. Kleven MD, Jue S, Enns CA. Transferrin receptors Tfr1 and Tfr2 bind transferrin through differing mechanisms. *Biochemistry*. 2018;57:1552–1559. doi:10.1021/acs.biochem.8b00006
34. Kawabata H. Transferrin and transferrin receptors update. *Free Radic Biol Med*. 2019;133:46–54. doi:10.1016/j.freeradbiomed.2018.06.037
35. Daniels TR, Delgado T, Rodriguez JA, Helguera G, Penichet ML. The transferrin receptor part I: biology and targeting with cytotoxic antibodies for the treatment of cancer. *Clin Immunol*. 2006;121:144–158. doi:10.1016/j.clim.2006.06.010
36. Gammella E, Buratti P, Cairo G, Recalcati S. The transferrin receptor: the cellular iron gate. *Metallomics*. 2017;9:1367–1375. doi:10.1039/c7mt00143f
37. Ponka P, Lok CN. The transferrin receptor: role in health and disease. *Int J Biochem Cell Biol*. 1999;31:1111–1137. doi:10.1016/s1357-2725(99)00070-9

38. Burnett JC, Henchal EA, Schmaljohn AL, Bavari S. The evolving field of biodefence: therapeutic developments and diagnostics. *Nat Rev Drug Discov*. 2005;4:281–297. doi:10.1038/nrd1694
39. Kedar U, Phutane P, Shidhaye S, Kadam V. Advances in polymeric micelles for drug delivery and tumor targeting. *Nanomedicine*. 2010;6:714–729. doi:10.1016/j.nano.2010.05.005
40. Shi J, Votruba AR, Farokhzad OC, Langer R. Nanotechnology in drug delivery and tissue engineering: from discovery to applications. *Nano Lett*. 2010;10:3223–3230. doi:10.1021/nl102184c
41. Kotta S, Aldawsari HM, Badr-Eldin SM, Nair AB, Yt K. Progress in polymeric micelles for drug delivery applications. *Pharmaceutics*. 2022;14:1636. doi:10.3390/pharmaceutics14081636
42. Aliabadi HM, Lavasanifar A. Polymeric micelles for drug delivery. *Expert Opin Drug Deliv*. 2006;3:139–162. doi:10.1517/17425247.3.1.139
43. Ayala-Mar S, Donoso-Quezada J, González-Valdez J. Clinical implications of exosomal Pd-L1 in cancer immunotherapy. *J Immunol Res*. 2021;2021:8839978. doi:10.1155/2021/8839978
44. Chen G, Huang AC, Zhang W, et al. Exosomal Pd-L1 contributes to immunosuppression and is associated with Anti-Pd-1 response. *Nature*. 2018;560:382–386. doi:10.1038/s41586-018-0392-8
45. Chen FF, Li Z, Ma D, Yu Q. Small-molecule Pd-L1 inhibitor Bms1166 abrogates the function of Pd-L1 by blocking its Er export. *Oncoimmunology*. 2020;9:1831153. doi:10.1080/2162402x.2020.1831153
46. Magiera-Mularz K, Kocik J, Musielak B, et al. Human and mouse Pd-L1: similar molecular structure, but different druggability profiles. *iScience*. 2021;24:101960. doi:10.1016/j.isci.2020.101960